NANO LETTERS

LETTER

pubs.acs.org/NanoLett

Signatures of Disorder in the Minimum Conductivity of Graphene

Yang Sui,*[,†,‡,∥] Tony Low,[†,§] Mark Lundstrom,[†,§] and Joerg Appenzeller[†,‡]

[†]School of Electrical and Computer Engineering, [‡]Birck Nanotechnology Center, [§]Network for Computational Nanoelectronics, Purdue University, West Lafayette, Indiana 47907, United States

Supporting Information

ABSTRACT: Graphene has been proposed as a promising material for future nanoelectronics because of its unique electronic properties. Understanding the scaling behavior of this new nanomaterial under common experimental conditions is of critical importance for developing graphene-based nanoscale devices. We present a comprehensive experimental and theoretical study on the influence of edge disorder and bulk disorder on the minimum conductivity of graphene ribbons. For the first time, we discovered a strong nonmonotonic size scaling behavior featuring a peak and saturation minimum conductivity. Through extensive numerical simulations and analysis, we are able to attribute these features to the amount of edge and bulk disorder in graphene devices. This study elucidates the quantum transport mechanisms in realistic experimental graphene systems, which can be used as a guideline for designing graphene-based nanoscale devices with improved performance.

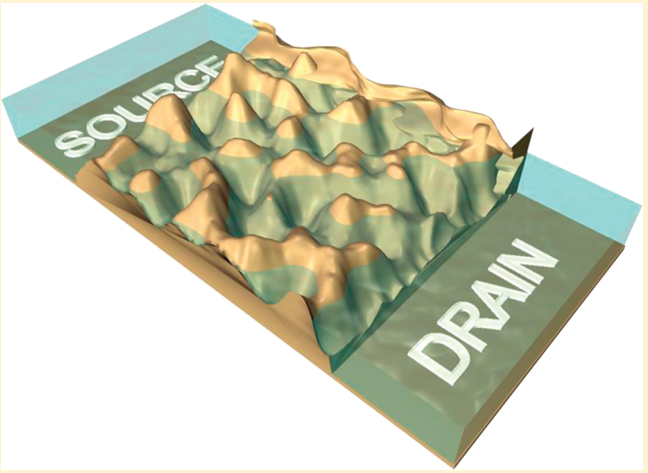

KEYWORDS: Graphene, minimum conductivity, disorder, edge states, evanescent, scaling

Conductivity of a material offers insights into the energy band structure and exhibits different behaviors depending on the scattering mechanisms involved. Conductivity is independent of geometry for conventional bulk materials, but scales with length for low-dimensional materials under ballistic transport conditions (e.g., carbon nanotubes),[1] where no scattering occurs within the channel. The situation becomes more intriguing for graphene at the Dirac point,[2−4] where the density of states (DOS) is zero. Despite zero carrier density, the conduction takes place by the evanescent modes tunnelling through the Dirac point and leads to a counterintuitive finite minimum conductivity (σ_{min}).[5,6] In the ideal disorder-free case, σ_{min} scales monotonically with the width-to-length ratio (W/L) of the channel.[6] In reality, disorder in experimental graphene structures has been found to be inevitable and profoundly impacts carrier transport,[7−9] particularly for the off-state. However, there has not been a comprehensive understanding on the scaling of σ_{min} over a broad width and length parameter space, where disorder dictates the transport behavior. Here, we report an experimental investigation of graphene ribbons in which σ_{min} is governed mainly by the impacts of edge and bulk disorder. In distinct contrast to the disorder-free case,[6,10] our investigation reveals a strong nonmonotonic W/L dependence along with an overall enhancement in σ_{min}, characterized by a peak and saturation. Our model for the disordered graphene system agrees quantitatively with the experiments. In addition, our framework accommodates previous findings[10] on minimum conductivity for graphene ribbons in different geometrical limits. This study probes into the behavior of disordered graphene system, elucidates the transport mechanism, and provides insights for improving the performance of graphene nanoelectronics.

Over the years, experiments have provided evidence that disorder significantly impacts the off-state carrier transport in graphene structures.[9] Minimum conductivity of graphene, initially thought to be a universal constant,[3,11,12] is only so when external perturbations such as disorder and most notably contacts are absent.[10,13−15] However, perturbations are ubiquitous for experimental graphene devices, and their impact on the finite size scaling of σ_{min} is unclear due to the lack of experimental data in the disorder dominated regime. To address this issue, we have fabricated bottom-gated graphene devices with dimensions larger than typical length scales of disorder[8] and covered a wide range of width-to-length ratio ($W/L = 0.1−2.6$). A two-probe setup rather than four-probe is employed since only the former explicitly accounts for the contacts, which are the origins of the evanescent modes and responsible for the observed width scaling behavior.[5,6]

Throughout this entire work, we focus on single-layer graphene devices on SiO_2/Si substrates. Figure 1a shows a scanning electron microscopy (SEM) micrograph of the structure under investigation. Typical transfer characteristics at different temperatures are shown in Figure 1b, where σ_{min} shows little temperature dependence. The width-to-length ratio is used as a metric to investigate the scaling behavior of σ_{min} (discussed in Supporting Information

Received: December 16, 2010

   dx.doi.org/10.1021/nl104399z | *Nano Lett.* XXXX, XXX, 000–000

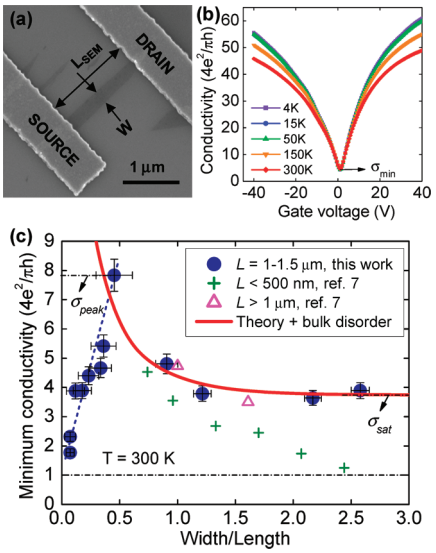

Figure 1. (a) SEM micrograph of a typical graphene device. (b) Transfer characteristics of a graphene device at T = 4−300 K. (c) Experimental observations of the geometrical scaling behavior of disordered graphene ribbons. The blue circles are our data from ribbons of various geometries, W = 0.1−4.9 μm and L = 1−1.5 μm. The green "+" and purple "Δ" are reproductions from a previous report.[10] The red solid curve indicates theory for disorder-free graphene ribbons[6] with the enhancement from bulk disorder.

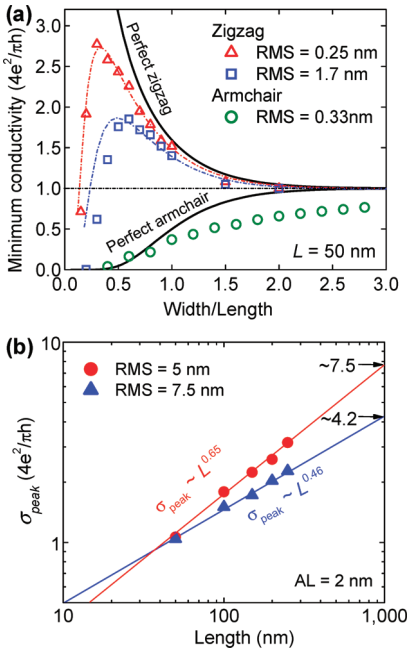

Figure 2. (a) Modeling results for σ_{min} in edge-disordered graphene ribbons. Symbols are from NEGF simulations for zigzag and armchair ribbons with different rms. AL = 1 nm. Dash-dotted lines are obtained analytically from eq 1 with α as a fitting parameter. The solid black curves are obtained from theory for disorder-free ribbons.[6] (b) Length scaling simulation for σ_{peak}. $W/L \approx 0.5$ and AL = 2 nm. Power-law extrapolation to L = 1 μm yields σ_{peak} = 7.5 and 4.2 ($4e^2/\pi h$) for rms = 5 and 7.5 nm, respectively. Note: The motivation for the length scaling study is that it is impractical to simulate live size devices (several μm) due to the limitation of computing power.

Supplement I) with the experimental findings shown in Figure 1c. Both the transfer length (L_T) and the contact resistance (R_C) are considered when evaluating L and σ_{min} (Supporting Information Supplement II). The following distinct features are immediately noticed: (i) σ_{min} has a nonmonotonic dependence on W/L with $\sigma_{peak} \sim 8$ ($4e^2/\pi h$) at $W/L \approx 0.5$; (ii) σ_{min} saturates for large W/L, denoted as $\sigma_{sat} \sim 4$ ($4e^2/\pi h$). Very few previous reports can be found on the geometrical scaling of σ_{min}. Figure 1c includes previous published data[10] "+" and "Δ" that exhibit an apparent monotonic scaling behavior, just as predicted for disorder-free graphene.[6] By studying devices much larger than typical dimensions of disorder and probing into a much broader W/L regime, we have uncovered new features in the scaling behavior of σ_{min}, characterized by σ_{peak} and σ_{sat}.

First, it is useful to recall that there are two types of states in a graphene ribbon, namely edge states and bulk states. Edge states are highly conductive propagating states residing along nonarmchair edges.[16−18] The conductance from edge states is independent of W, and therefore would dominate as W/L approaches zero and lead to a diverging σ_{min}.[6] Bulk states on the other hand are less conductive evanescent states with the number of states proportional to W. In the large W/L regime, bulk states dominate the transport and lead to a constant σ_{min} of $4e^2/\pi h$ in the disorder-free case.[5,6] Combining these two types of states is the key to understand the experimental observations. Note that both types of states are involved in transport through zigzag ribbons, whereas only bulk states are responsible for transport in armchair ribbons.

Edge disorder is a result of the inevitable edge roughness from imperfect cleaving or top-down fabrication. It is known to cause gaplike transport behavior due to localization or quantum dot formation.[19−22] A zigzag edge is more common for graphene ribbons than an armchair edge since ribbons with edges "between" zigzag and armchair tend to acquire zigzag-type boundaries.[16] In the absence of disorder, σ_{min} is predicted to increase or decrease monotonically with W/L for armchair or zigzag ribbons[6] (black curves in Figure 2a). We have performed quantum transport simulations using a non-equilibrium Green's function (NEGF) formalism to model the edge and bulk disorder in 2D graphene sheets with the numerical implementations described in Supporting Information Supplement IV and V. All simulations are performed for T = 0 K (see Supporting Information Supplement III). Indeed, edge disorder immediately gives rise to a nonmonotonic behavior for zigzag ribbons, while σ_{min} for armchair ribbons remains monotonic as a function of W/L, albeit with a lower conductivity (Figure 2a). Interestingly, our experimental devices (Figure 1c) exhibit a scaling behavior that is consistent only with edge-disordered zigzag ribbons, and none of the devices fall into the "armchair" trend as predicted by the green circles in Figure 2a. This observation can be viewed as a manifestation of the fact that the zigzag boundary condition, where the edge is characterized by a majority sublattice and hence accommodates edge states, is generic for experimental graphene ribbons.

An analytical description for the impact of edge disorder can be obtained by considering a width-dependent transport gap. σ_{min} for a zigzag ribbon with edge roughness can be described as follows[6]

$$\sigma_{min} = \frac{\pi L}{W}\left[\sum_{n=2}^{\infty} \cosh^{-2}\left(\frac{n\pi}{W}L\right) + \frac{1}{2}\cosh^{-2}\left(\frac{\varepsilon_{loc}}{\hbar v_f}L\right)\right] \quad (1)$$

given in units of $4e^2/\pi h$. $\varepsilon_{loc} = \alpha/W^{\beta}$ is the Anderson localization-induced transport gap with $\alpha \sim 1$ ÅeV and $\beta \sim 1$, as estimated in ref 20. Although temperature should have an effect on ε_{loc} due to dephasing, however, the thermal broadening due to Fermi function

dx.doi.org/10.1021/nl104399z |Nano Lett. XXXX, XXX, 000–000

smearing is negligible as discussed in Supporting Information Supplement III. Since ε_{loc} increases with decreasing width, σ_{min} for narrow ribbons is more strongly suppressed than for wide ribbons, resulting in decreasing σ_{min} values for small W/L. Furthermore, the edge states wave function decays exponentially from the edges with a characteristic length proportional to W at a given Fermi energy (E_F),[23] making the narrower ribbons more susceptible to edge disorder. Another way to form a transport gap in graphene nanoribbons (GNRs) is to combine small confinement-induced energy gaps with potential inhomogeneities.[19,21,22] We believe that the transport gap in our case is mainly due to edge localization for the following reasons: First, the smallest W (~100 nm) is much larger than the effective diameter of a charging island (~20 nm) near the Dirac point[8] and is unlikely to form isolated quantum dots. Second, the confinement-induced energy gap for $W \geq 100$ nm is too small to block the band-to-band tunnelling current. Therefore, it is likely that edge roughness scattering is responsible for σ_{min} reduction for zigzag ribbons of small W/L. The length scaling of σ_{peak} is found to follow a power-law relationship, as shown in Figure 2b. Extrapolation to $L = 1$ μm yields $\sigma_{peak} \approx 4.2$ ($4e^2/\pi h$) for reasonable assumptions of root-mean-square edge roughness (rms = 7.5 nm) and autocorrelation length (AL = 2 nm).[24,25] Note that since the peak position (not the peak height) is roughly a constant when the rms roughness is varied, we deduce that $\sigma_{peak} \propto W^{0.46}$ (as $W/L \approx$ constant at the peaks), a finding that will become relevant in subsequent discussions.

Bulk disorder in graphene arises from charge inhomogeneity at the graphene−substrate interface, with a typical potential fluctuation of ±40 meV,[8] the origin of which could be due to charge impurities on SiO_2. Local electron- and hole-rich regions, called electron−hole puddles, are induced in graphene with typical diameters of ~150 nm.[8] For any given E_F line-up in the off-state, percolation paths exist from the source to the drain through connected electron and hole puddles. As a result, current flows preferably through the regions of unperturbed potential to avoid the additional resistance associated with the pn interfaces at puddle boundaries,[26] as demonstrated by Figure 3a. Therefore, bulk disorder has a strong influence on σ_{min}.

Figure 3b shows the NEGF simulation results for σ_{min} versus W/L for ribbons with bulk disorder. Adding bulk disorder to graphene leads to higher conductivity,[27] which is exactly the opposite trend compared to other material systems. The reason for this unique behavior lies in the fact that graphene is a gapless material, where carriers can tunnel almost unimpeded from the conduction band into the valence band. Different E_F line-ups with respect to the Dirac point lead to a variation of DOS and thus conductivity in different puddles. The average DOS in the puddles increases as the magnitude of bulk disorder increases due to the linear energy dispersion of graphene. This leads to an enhancement in σ_{min} with increasing bulk disorder over the entire W/L range (Figure 3b). Effective medium theory is able to capture the main features of this phenomenon (Figure 3c), with equations in Supporting Information Supplement VI. It is a remarkable coincidence that the saturation feature of the bulk states conductivity persists for both disorder-free and bulk-disordered ribbons, despite different mechanisms involved. The former is due to evanescent transport, while the latter is dominated by percolation. For smaller devices (e.g., $L < 500$ nm) that only contain a few puddles, the potential is relatively uniform across the channel and the impact of bulk disorder is minimal. As a result, σ_{min} is markedly lower than for large devices,[10] just like the disorder-free case[6] (e.g., "+" in Figure 1c). Using the effective

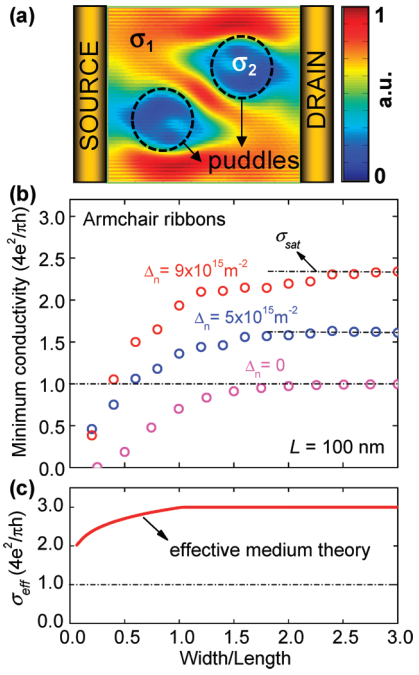

Figure 3. (a) Current density in a graphene channel with two puddles (marked by circles). σ_1 and σ_2 indicate regions of high and low conductivity. (b) Modeling results for σ_{min} in bulk-disordered graphene ribbons. Symbols are from NEGF simulations for different charge density fluctuations (Δ_n). Armchair ribbons are used, but the results can be extended to all types of ribbons. $L = 100$ nm, $\mu_R = 3$ nm, rms ~ 0.25 nm, and AL ~ 1 nm. (c) σ_{eff} vs W/L according to the effective medium model (equations in Supporting Information Supplement VI).

medium model, we obtain an effective conductivity $\sigma_{eff} \propto W^{0.16}$ for $W/L < 1$, assuming $\sigma_1/\sigma_2 = 0.01$ and $L \approx 30$ μ_R (puddle radius). Rigorous NEGF simulations assuming reasonable bulk disorder parameters extrapolate to $\sigma_{sat} \approx 4.3$ ($4e^2/\pi h$) for $L = 1$ μm. Quantitative agreement between experiments and NEGF simulations for the peak and saturation σ_{min} is reached with details in Supporting Information Supplement VII.

Finally, we discuss the implications of this work for nanoscale graphene devices. It is a major hurdle to realize high-performance graphene transistors due to the absence of a bandgap. Our study provides valuable insights in this context. Figure 4a shows the width scaling of the on- and off-state conductance (G_{on} and G_{off}). Interestingly, while $G_{on} \propto W$, G_{off} follows an unconventional trend $G_{off} \propto W^{1.3}$. We attribute this stronger suppression in G_{off} as W decreases to the following mechanisms: (i) the number of rough edges per unit width is increased, thereby suppressing the highly conductive edge states; (ii) some percolation paths are terminated. The particular $G_{off}-W$ dependence can be rationalized knowing $\sigma_{min} \propto W^{0.16-0.46}$ for $W/L < 0.5$ and $G_{off} = \sigma_{min}(W/L) \propto W^{1.16-1.46}$. Width reduction without compromising the on-current can be accomplished by cutting nanometer-scale incisions along the transport direction (Figure 4b). We have observed at least a two- to three-fold improvement in on/off ratio by moderately reducing the effective width from 1 μm to 100 nm, as demonstrated in Figure 4a. This also allows us to scale the channel width without modifying the on/off ratio to facilitate circuit level design requirements. In a similar fashion, the recently demonstrated graphene nanomesh works under the same principle and was found to achieve an on/off ratio of ~160.[28] Exploiting these geometries will allow designing better

dx.doi.org/10.1021/nl104399z |Nano Lett. XXXX, XXX, 000–000

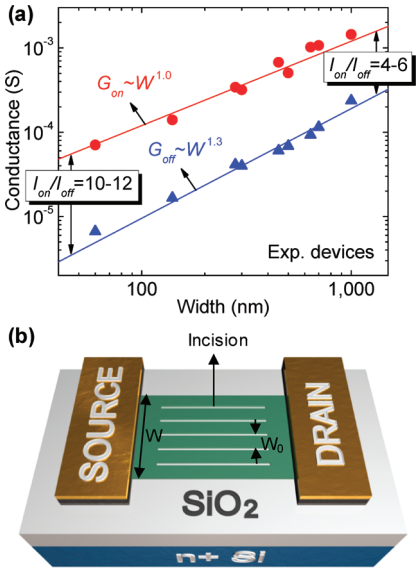

Figure 4. (a) Experimental observations of on-state and off-state conductance (G)−width scaling. $L \sim 2$ μm and $W/L \leq 0.5$ for all devices, belonging to the ascending trend in Figure 1c. (b) Structure of a proposed graphene transistor with mesoscopic incisions for improved on/off ratio and scalability.

graphene-based nanoelectronics such as RF devices and biosensors.[29,30]

Note: Our study should have relevance to the recently demonstrated atomically flat graphene on boron nitride system.[31] In fact, we expect a stronger nonmonotonic dependence of σ_{min} as a function of W due to suppression of bulk disorder in such a system.

Methods. Graphene flakes are mechanically exfoliated onto 90 nm SiO_2/Si substrates from highly oriented pyrolytic graphite (HOPG, NT-MDT). Source and drain contacts are patterned by e-beam lithography, followed by e-beam evaporation and lift-off of a stack of Ti/Pd/Au (10 nm/30 nm/20 nm) metals. To prevent damages to the graphene ribbons from the e-beam patterning process, we choose graphene flakes of various widths and lengths as naturally cleaved from the exfoliation process. In this way, there are no further modifications on the graphene ribbons widths. Devices with W = 0.1−4.9 μm and physical lengths (L_{SEM}) of 1.0−1.5 μm are created from single-layer graphene flakes. The thickness of the graphene flakes is determined by optical analysis and atomic force microscopy (AFM). Electrical measurements of the devices are carried out at T = 4−300 K under vacuum (1×10^{-7} Torr). The field-effect mobility of typical devices is ~4000 $cm^2/(V\,s)$ as determined from room temperature transfer characteristics.

■ ASSOCIATED CONTENT

Supporting Information. A detailed description of the experiments and simulations are available. This material is available free of charge via the Internet at http://pubs.acs.org.

■ AUTHOR INFORMATION

Corresponding Author

*E-mail: suiyang2000@gmail.com.

Present Address

‖GE Global Research Center, Niskayuna, NY 12309, United States.

■ ACKNOWLEDGMENT

The authors thank S. Datta, M. Alam, Z. Jacob, and F. Guinea for discussions and J. T. Smith for assistance with the graphics. The work was supported by INDEX (NRI) and Intel Corp. with computational resources from NCN.

■ REFERENCES

(1) Javey, A.; Guo, J.; Wang, Q.; Lundstrom, M.; Dai, H. J. *Nature* **2003**, *424*, 654.
(2) Novoselov, K. S.; Geim, A. K.; Morozov, S. V.; Jiang, D.; Zhang, Y.; Dubonos, S. V.; Grigorieva, I. V.; Firsov, A. A. *Science* **2004**, *306*, 666.
(3) Novoselov, K. S.; Geim, A. K.; Morozov, S. V.; Jiang, D.; Katsnelson, M. I.; Grigorieva, I. V.; Dubonos, S. V.; Firsov, A. A. *Nature* **2005**, *438*, 197.
(4) Zhang, Y. B.; Tan, Y. W.; Stormer, H. L.; Kim, P. *Nature* **2005**, *438*, 201.
(5) Katsnelson, M. I. *Eur. Phys. J. B* **2006**, *51*, 157.
(6) Tworzydlo, J.; Trauzettel, B.; Titov, M.; Rycerz, A.; Beenakker, C. W. J. *Phys. Rev. Lett.* **2006**, *96*, No. 246802.
(7) Sui, Y.; Appenzeller, J. *Nano Lett.* **2009**, *9*, 2973.
(8) Martin, J.; Akerman, N.; Ulbricht, G.; Lohmann, T.; Smet, J. H.; Von Klitzing, K.; Yacoby, A. *Nat. Phys.* **2008**, *4*, 144.
(9) Neto, A. H. C.; Guinea, F.; Peres, N. M. R.; Novoselov, K. S.; Geim, A. K. *Rev. Mod. Phys.* **2009**, *81*, 109.
(10) Miao, F.; Wijeratne, S.; Zhang, Y.; Coskun, U. C.; Bao, W.; Lau, C. N. *Science* **2007**, *317*, 1530.
(11) Khveshchenko, D. V. *Phys. Rev. Lett.* **2006**, *97*, No. 036802.
(12) Nomura, K.; MacDonald, A. H. *Phys. Rev. Lett.* **2007**, *98*, No. 076602.
(13) Tan, Y. W.; Zhang, Y.; Bolotin, K.; Zhao, Y.; Adam, S.; Hwang, E. H.; Das Sarma, S.; Stormer, H. L.; Kim, P. *Phys. Rev. Lett.* **2007**, *99*, No. 246803.
(14) Geim, A. K.; Novoselov, K. S. *Nat. Mater.* **2007**, *6*, 183.
(15) Chen, J. H.; Jang, C.; Adam, S.; Fuhrer, M. S.; Williams, E. D.; Ishigami, M. *Nat. Phys.* **2008**, *4*, 377.
(16) Akhmerov, A. R.; Beenakker, C. W. J. *Phys. Rev. B* **2008**, *77*, No. 085423.
(17) Kobayashi, Y.; Fukui, K.; Enoki, T.; Kusakabe, K.; Kaburagi, Y. *Phys. Rev. B* **2005**, *71*, No. 193406.
(18) Fujita, M.; Wakabayashi, K.; Nakada, K.; Kusakabe, K. *J. Phys. Soc. Jpn.* **1996**, *65*, 1920.
(19) Gallagher, P.; Todd, K.; Goldhaber-Gordon, D. *Phys. Rev. B* **2010**, *81*, No. 115409.
(20) Mucciolo, E. R.; Neto, A. H. C.; Lewenkopf, C. H. *Phys. Rev. B* **2009**, *79*, No. 075407.
(21) Sols, F.; Guinea, F.; Neto, A. H. C. *Phys. Rev. Lett.* **2007**, *99*, No. 166803.
(22) Han, M. Y.; Brant, J. C.; Kim, P. *Phys. Rev. Lett.* **2010**, *104*, No. 056801.
(23) Brey, L.; Fertig, H. A. *Phys. Rev. B* **2006**, *73*, No. 235411.
(24) Gupta, A. K.; Russin, T. J.; Gutierrez, H. R.; Eklund, P. C. *ACS Nano* **2009**, *3*, 45.
(25) Tapaszto, L.; Dobrik, G.; Lambin, P.; Biro, L. P. *Nat. Nanotechnol.* **2008**, *3*, 397.
(26) Cheianov, V. V.; Fal'ko, V. *Phys. Rev. B* **2006**, *74*, No. 041403.
(27) Bardarson, J. H.; Tworzydlo, J.; Brouwer, P. W.; Beenakker, C. W. J. *Phys. Rev. Lett.* **2007**, *99*, No. 106801.
(28) Bai, J.; Zhong, X.; Jiang, S.; Huang, Y.; Duan, X. *Nat. Nanotechnol.* **2010**, *5*, 190.
(29) Lin, Y. M.; Dimitrakopoulos, C.; Jenkins, K. A.; Farmer, D. B.; Chiu, H. Y.; Grill, A.; Avouris, P. *Science* **2010**, *327*, 662.
(30) Schedin, F.; Geim, A. K.; Morozov, S. V.; Hill, E. W.; Blake, P.; Katsnelson, M. I.; Novoselov, K. *Nat. Mater.* **2007**, *6*, 652.
(31) Dean, C. R.; Young, A. F.; Meric, I.; Lee, C.; Wang, L.; Sorgenfrei, S.; Watanabe, K.; Taniguchi, T.; Kim, P.; Shepard, K. L.; Hone, J. *Nat. Nanotechnol.* **2010**, *5*, 722.